

pubs.acs.org/JPCC Article

Tenth-Order Multiphoton Excitation and Saturable Second Harmonic Generation in Polyoxometalate-Exfoliated Molybdenum Disulfide

Published as part of The Journal of Physical Chemistry virtual special issue "Honoring Michael R. Berman". Megan A. Steves, Ali Jawaid, Ariel Struzyk, Riccardo Torsi, Joshua A. Robinson, Richard A. Vaia, and Kenneth L. Knappenberger, Jr.*



Cite This: J. Phys. Chem. C 2022, 126, 18036-18046



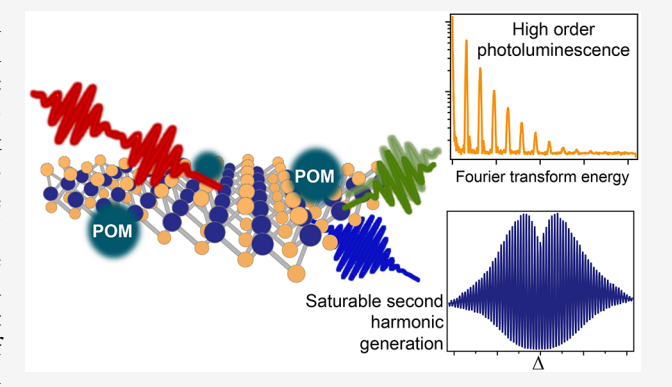
ACCESS

Metrics & More

Article Recommendations

s) Supporting Information

ABSTRACT: Nanomaterials are promising alternatives to traditional bulk crystals for nonlinear optics and energy conversion materials. In this study, we report the observation of saturable second harmonic generation and high-order (up to 10th) multiphoton photoluminescence in colloidal MoS₂ nanoflakes prepared by redox exfoliation which generates polyoxometalate clusters. Fourier transform nonlinear optical spectroscopy enabled the resolution of these high-order signals through two-dimensional nonlinear excitation/detection correlation spectra. Complementary modeling of the nonlinear interferograms suggested mechanisms for the observed high-order signals, which involve saturation of transitions resonant with the harmonic energy and multiple competing orders of multiphoton absorption. The saturable second harmonic generation and high-order multiphoton photoluminescence, which were not



observed in MoS₂ prepared by chemical vapor deposition, are related to the formation of polyoxometalate clusters during the redox exfoliation process. Further studies demonstrated that polyoxometalates can induce high-order nonlinear optical effects in other colloidal semiconductors with resonances at the harmonic energy, suggesting a general route to drastically alter the nonlinear optical response of nanomaterials with molecular adsorbates. This response is due in part to the interfacial charge transfer between polyoxometalate species and the nanomaterial. Fourier transform nonlinear optical spectroscopy offers a route to resolving the effects of molecular adsorbates, which are obscured in traditional nonlinear optical measurements.

INTRODUCTION

Nonlinear optical effects arising from the interaction of intense laser fields with matter, such as harmonic generation and multiphoton absorption, are key to modern technologies including frequency conversion, photolithography, and bioimaging.⁴ Low-dimensional nanomaterials including transition metal dichalcogenides (TMDs) and quantum dots are desirable for nonlinear optics because phase matching conditions required for nonlinear transduction in bulk materials are generally relaxed for these systems. Additionally, quantum-confined materials often exhibit intrinsically strong light-matter interactions that can be used to increase nonlinear optical signal strengths. Facile incorporation of low-dimensional nanostructures into multicomponent heterostructures allows flexibility for tuning the optical and electronic properties of composite materials. Robust solution-phase nucleation and exfoliation has expanded the range of low-dimensional materials that can be used for applications in nonlinear optics.

Polyoxometalates (POMs) are a class of macro-ionic metal oxide clusters which are highly redox reactive and have been used in hybrid materials for photocatalysis and electro-chemistry, ^{5,6} as well as for redox synthesis of nanoparticles and layered materials, including TMDs. ^{7–9} The charge-transfer properties of polyoxometalates have also been exploited to increase the hyperpolarizability of POM—organic molecular hybrids. ^{10,11} Previous reports have shown that POM clusters are natively present in many TMD systems as surface oxidative byproducts. ^{9,12} However, to date, their effect on the nonlinear optical properties of nanomaterials has not been investigated.

Received: August 10, 2022 Revised: October 4, 2022 Published: October 18, 2022





Here we show that doping with polyoxometalates can induce saturable second harmonic generation (SHG) and up to 10thorder multiphoton absorption in colloidal semiconducting nanocrystals and nanoflakes. These high-order perturbative nonlinear optical effects, which are obscured in conventional steady-state, power-dependent nonlinear optical measurements, are revealed using Fourier transform nonlinear optical spectroscopy (FT-NLO). Our results imply that charge transfer to the adsorbed molecular species and a two-photon resonance in the semiconductor contribute to the observed high-order nonlinear optical effects. While previous studies have demonstrated that improvements in nonlinear optical yields can be achieved through molecular doping and functionalization of semiconducting nanocrystals and TMDs, 13-16 these results demonstrate that polyoxometalate clusters can allow new nonlinear optical processes to be observed due, in part, to interfacial charge transfer. Given the ubiquity of POMs for redox chemistry, these results signify their importance in determining the nonlinear optical response of nanomaterials. Beyond nonlinear optical applications, our results implicate interfacial charge transfer, which should impact the electrochemical, catalytic, and reactivity characteristics of material heterostructures.

In this study we report on the high-order nonlinear optical properties of redox-exfoliated transition metal dichalcogenides (TMDs), which have received attention as candidates for use in photonic devices due to their linear and nonlinear optical properties, including strong exciton absorption, saturable absorption, direct bandgap photoluminescence, and valleyselective excitation. ^{17–20} TMDs, particularly MoS₂, have also been noted as efficient materials for second harmonic generation (SHG).21 This SHG response is affected by the intrinsic symmetry breaking of MoS2 with an odd number of layers along with resonance of the harmonic with the C-peak observed in the optical absorption spectrum, which can result in sheet second-order nonlinear susceptibilities $(\chi^{(2)})$ in the range of 0.1-1 nm²/V.²² In addition to the C resonance, which is attributed to band nesting around the Γ point of the Brillion zone, the extinction spectrum of MoS₂ exhibits a broad peak at 3.1 eV corresponding to the D resonance, which has been suggested to arise from transitions between van Hove singularities at the M point of the Brillion zone (Figure S1a).²³ These transitions which are resonant with the second harmonic can be saturated, leading to the saturable SHG effect observed in this work.

While most previous studies of these nonlinear optical properties have focused on TMDs prepared through bottom-up approaches, solution-phase preparation of TMDs offers the advantage of easy integration with existing manufacturing technologies. Redox-exfoliation of TMDs provides a low-cost, scalable method to generate colloidally stable few-layer and monolayer TMDs with generality and high yield. However, few studies thus far have examined the linear and nonlinear optical properties of redox-exfoliated TMDs. As we demonstrate in this study, the POM clusters produced during the redox-exfoliation process have a profound effect on the nonlinear optical properties of TMDs. As a result, redox-exfoliated TMDs of MoS₂ and WS₂ exhibit saturable SHG and high-order multiphoton photoluminescence (MPPL) as demonstrated in this work.

In this work, we demonstrate that redox-exfoliated MoS_2 exhibits previously unobserved high-order nonlinear optical effects which are uniquely resolved through FT-NLO. Analysis

of the time-domain interferograms and comparison with simulated results implicate saturable SHG and high-order MPPL as responsible for these effects. Based on the nonlinear emission spectra of these systems and examination of other POM/nanomaterial systems, we discuss mechanisms of the high-order nonlinearities involving charge transfer to the POMs and two-photon resonances in the semiconductor. These effects are generalizable to other colloidal semiconductors interfaced with POMs, and highlight the important influence of surface-adsorbed molecules on material nonlinear optical properties. The FT-NLO method also provides a route to probing and understanding intercomponent charge transfer in heterostructures, which will affect their electrochemical and catalytic properties.

METHODS

Synthesis. Previously described synthesis protocols were used to prepare redox-exfoliated $MoS_2^{9,12}$ and MOCVD $MoS_2^{27,28}$ H-bn flakes in solution were purchased from 2D Semiconductors. Solution phase samples were drop cast onto a glass coverslip for measurement.

FT-NLO Experiments. As described previously,²⁹ the 800 nm fundamental beam from a Ti:sapphire oscillator (Coherent, Vitara) was directed through the pulse replica generator described in the text, and focused onto the sample with a 0.23 NA aspheric lens. The nonlinear emission was collected with a 1.25 NA oil immersion objective (Amscope) and separated from the fundamental with a 680 nm long pass filter. The nonlinear signal was detected with a spectrograph/EMCCD (Andor, Shamrock 303i/iXon).

FT-NLO data analysis and simulations were performed using home-written scripts for Igor Pro. Background and details of the density matrix approach used is given in the Supporting Information. Simulations were performed with a carrier wavelength of 800 nm and a pulse duration of 20 fs. A dephasing time of 10 fs and a nonradiative relaxation time constant of 50 fs was used for all states. A radiative relaxation time constant of 500 ps was used for state 1, as described in the text.

RESULTS

Fourier Transform Nonlinear Optical Spectroscopy of MoS₂. We begin by describing how FT-NLO microscopy was used reveal the high-order nonlinear excitation spectra of redox-exfoliated MoS₂. Our experimental method for FT-NLO has been described previously, ^{29,30} and is depicted in Figure S1b,c. The measurement is centered around a broad bandwidth Ti:sapphire oscillator, which induces NLO signals that are collected with a high numerical aperture objective and directed to a spectrograph/EMCCD for detection (Figure S1b). For interferometric measurements, a pulse replica generator is used to generate phase-stable and temporally separated laser pulse pairs (Figure S1c). Briefly, the parent pulse generated by the Ti:sapphire oscillator is polarized at 45° with respect to the lab frame and passes through a pulse replica generator consisting of a series of birefringent α -BBO wedges which separates the pulse into x- and y-polarized components and introduces a time delay, $\Delta \tau$. A polarizer projects both pulses back into the same polarization plane and the pulse pair is used to generate nonlinear signal.

The nonlinear signal can be imaged as a function of $\Delta \tau$, and Fourier transformed along $\Delta \tau$ in order to spatially resolve the

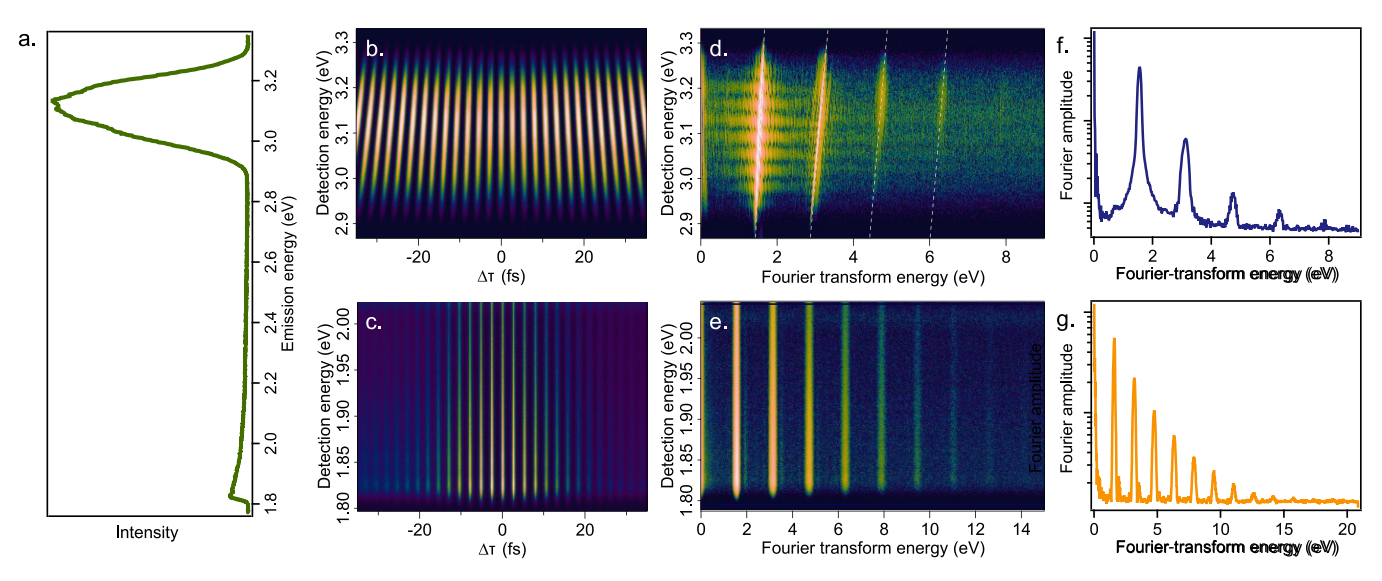


Figure 1. Fourier-transform nonlinear optical spectroscopy of redox-exfoliated MoS_2 . (a) nonlinear emission spectrum from MoS_2 excited with 1.55 eV fundamental. (b, c) Spectrally resolved interferograms centered at 3.1 (b) and 1.9 eV (c) detection energies. (d, e) Excitation/detection correlation maps obtained by Fourier-transform of the data in panels b and c. (f) Fourier transform spectra in panel d integrated from 2.9 to 3.3 eV detection energy. (g) Fourier transform spectra in panel e integrated from 1.8 to 2.0 eV detection energy.

resonance response of the sample.²⁹ Alternatively, the nonlinear signal can be dispersed by a spectrograph in order to collect the nonlinear emission spectra at each interpulse time delay. The resultant spectrally resolved interferometric data from a coherent nonlinear signal is equivalent to an interferometric frequency-resolved optical gating (IFROG) trace from a resonant sample. 31 A Fourier transform along $\Delta \tau$ results in a two-dimensional excitation/detection frequency correlation. The 2D spectrum can be used to differentiate parametric signals such as harmonic generation from incoherent signals such as multiphoton photoluminescence.³² While nonparametric, incoherent multiphoton photoluminescent emission is not correlated with the excitation energy, coherent harmonic generation signals are characterized by a correlation between the excitation and detection frequencies manifesting as a diagonal signal on the 2D frequency map. The range and resolution of the excitation frequency axis in the 2D maps are determined by the sampling rate and the maximum value of $\Delta \tau$, respectively. In this study, increments of $\Delta \tau$ of approximately 100 as were used, allowing energies over 20 eV to be resolved. The total range of $\Delta \tau$ sampled resulted in a spectral resolution of approximately 20 meV.

The nonlinear emission spectrum of MoS₂ shown in Figure 1a is dominated by a second harmonic generation (SHG) peak at ~3.1 eV and a broad emission at lower energies which is attributed to multiphoton photoluminescence (MPPL). Collecting this spectrum as a function of $\Delta \tau$ yields the spectrally resolved interferogram shown in Figure 1b,c. The excitation/detection correlation map obtained by Fourier transform along τ is shown in Figure 1d,e. We focus on the ranges between 1.80-2.05 and 2.85-3.35 eV in the detection spectrum as representative of MPPL and SHG emission, respectively. As expected, harmonic generation and photoluminescence signals are distinguishable based on their excitation/detection correlations. At 3.1 eV detection energy, the parametric signals are diagonally distributed along the excitation/detection frequency correlation map (i.e., detection energy = 2 · excitation energy and detection energy = excitation

energy), which are indicated in Figure 1d as dashed lines. This supports the attribution of the peak at 3.1 eV as second harmonic generation. The broader emission extending to lower energies, however, has no correlation with the excitation energy, manifesting as a vertical signal in the 2D excitation/detection maps. This uncorrelated signal is consistent with incoherent, nonparametric emission from MPPL.

The excitation spectrum of MoS_2 exhibits peaks at several multiples of ω , the fundamental energy, reflecting different orders of the nonlinear signal. This can be demonstrated by considering the time-domain signal integrated over a range of detection energies, which is equivalent to the interferometric autocorrelation. The interferometric autocorrelation resulting from an n^{th} -order nonlinear process excited by a pulse with electric field E(t) is given by

$$IAC^{(n)}(\tau) = \int_{-\infty}^{\infty} |\{E(t) + E(t+\tau)\}^n|^2 dt$$
 (1)

The interferometric autocorrelation will contain terms oscillating at 1ω , 2ω , ..., $n\omega$. Figure 1f,g shows the excitation spectra for SHG and MPPL emission obtained by integrating the signal between detection energies of 2.90 to 3.30 eV for SHG and 1.80 to 2.02 eV for MPPL. The SHG excitation spectra exhibits peaks at 1ω , 2ω , 3ω , and 4ω . The 1ω and 2ω peaks are consistent with expectations for a second-order nonlinear signal, such as SHG. The additional peaks at 3ω and 4ω are unexpected for emission arising from SHG. The origins of these additional peaks will be discussed below. The MPPL excitation spectra also exhibits peaks at multiples of ω , extending past 10ω , or 15 eV. The presence of these peaks in the nonlinear excitation spectrum suggests high-order multiphoton absorption generates the excited carriers which eventually radiatively decay to yield the broad photoluminescence observed in the nonlinear emission spectrum (Figure 1a).

At first, these high-order nonlinearities in the FT spectra appear inconsistent with the fluence-dependence of the nonlinear signals. The SHG and MPPL intensity were

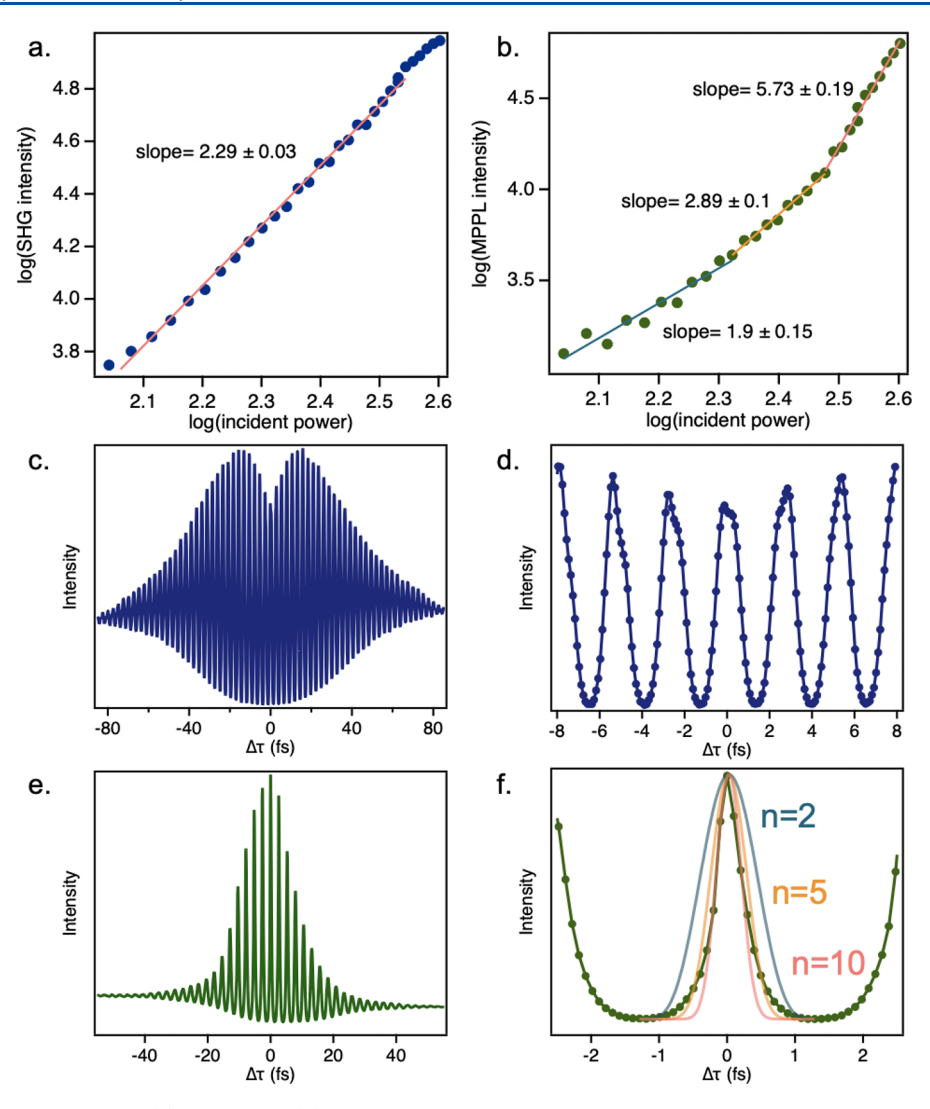


Figure 2. Power dependence of SHG (a) and MPPL (b) signals in redox-exfoliated MoS₂. Time-domain interferograms showing the intensity of the SHG (c, d) and MPPL (e, f) signals as a function of interpulse time delay with an average excitation power of approximately 4 MW/cm². Modeling results for 2- (blue), 5- (orange), and 10-photon (pink) absorption are shown in panel (f). The experimental data is shown in green.

measured as a function of the excitation power (Figure 2a,b). For a perturbative nonlinear process, the photon order n can be obtained by fitting the measured nonlinear intensity, $I_{\rm NLO}$, to $I_{\rm NLO} = I_{\rm ex}^{\ \ n}$, where $I_{\rm ex}$ is the excitation intensity. In Figures 2a,b, the $log(I_{NLO})$ is plotted versus $log(I_{ex})$, which should have a linear relationship with slope n. For the SHG signal, we obtain $n = 2.29 \pm 0.03$ over most of the incident intensity range, which is close to the expected value of 2. At high pump fluences, the SHG power dependence deviates from the expected quadratic behavior. For the PL, however, the signal power dependence cannot be described by a power law fit with a single photon order n. From the data we obtain n ranging from 1.9 \pm 0.15 at low $I_{\rm ex}$ up to 5.7 \pm 0.19 at high $I_{\rm ex}$. Thus, the harmonic peaks at $3-4\omega$ and $6-10\omega$ in the SHG and MPPL Fourier transform spectra, respectively, are not explained by the steady-state power-dependent data.

We next focus on understanding the unexpected higherorder nonlinearities, beginning with the SHG FT spectrum. The peaks at 3ω and 4ω excitation energies are distributed diagonally in the 2D detection-excitation correlation map (Figure 1d), indicating that they do not arise from overlapping SHG and MPPL signals. However, these peaks have a slope of approximately 1, which indicates that they do not arise from third or fourth harmonic generation, which would have a slope of 2/3 or 1/2, respectively. The time-domain interferograms (Figure 2c,d) offer insights into the origins of the 3ω and 4ω peaks. The envelope of the SHG-detected interferogram exhibits a decrease in intensity around zero interpulse delay (Figure 2c). This is in contrast with the envelope of the MPPL interferogram, which exhibits a maximum at τ_0 (Figure 2e). A closer look at the SHG interferogram also reveals asymmetries in the oscillating signal, which are not present in the MPPL interferogram (Figure 2d,f).

Next, we investigate the power dependence of these unexpected nonlinearities in the interferometric SHG signal. Figure S2a shows the SHG interferogram from redox-exfoliated MoS₂ under different average excitation fluences. The fluences indicated in the legend correspond to the average fluence for long interpulse delays; at τ_0 , constructive interference of the two pulses will result in fluences of nearly $10~\mathrm{MW/cm^2}$. From Figure S2a it is apparent that the decrease in signal around τ_0 occurs only at high fluences; the third and fourth peaks in the FT spectra also become more prominent at higher fluences (Figure S2b). The observation of the decrease

in signal around time zero suggests that a saturation of the SHG signal at high fluences is involved in the peaks at 3ω and 4ω in the SHG FT-spectrum.

As described above, the MPPL interferogram of redoxexfoliated MoS₂ does not demonstrate the same features as the SHG interferogram. As shown in Figure 2e,f, the envelope of the interferogram peaks at τ_0 , and the interference peaks around τ_0 are symmetric with respect to time. There is an overall decrease in the signal intensity at positive time delays; this is attributed to sample photodegradation likely occurring around τ_0 , where the excitation fluence is highest. As shown in eq 1 above, the exact form of the interferometric autocorrelation is determined by the specific characteristics of the pulse. However, between $\tau = \frac{1}{2\omega}$ to $\frac{1}{2\omega}$ the interferogram can be modeled as $I_{\rm NLO} = (\cos \omega \tau)^{2n}$. Figure 2f compares the anticipated lineshapes for n = 2, 5, and 10. It is apparent that no single photon-order n can accurately fit the experimental data. While the n = 2 trace most closely reproduces the signal at approximately $\tau = \pm \frac{1}{2\omega}$ ($\tau = \pm 1.3$ fs), where destructive interference of the pulse pair leads to lower fluences, at $\tau = 0$ the signal is more closely matched by a n = 10 dependence.

Modeling the Nonlinear Response of MoS₂. To obtain more insight into the mechanism responsible for generating the high-order nonlinearities observed in the SHG and MPPL from redox-exfoliated MoS₂, modeling of the interferometric signal of a four-level system was performed using a density matrix approach. A schematic of the four-level model system used to simulate the interferometric response is shown in Figure 3. In this model, states $|0\rangle$ and $|2\rangle$ are connected by a

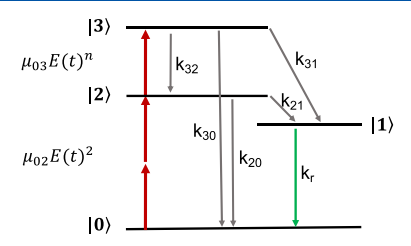


Figure 3. Schematic illustrating the four-level system described in the text.

two-photon interaction, while state $|3\rangle$ is coupled to the ground state by an n-photon interaction, where n is an adjustable parameter. Because peaks up to 10ω were observed in the experimental FT spectra, n=10 was chosen for these simulations. Once excited, carriers in $|2\rangle$ ($|3\rangle$) can relax to state $|1\rangle$ with rates k_{21} (k_{31}) or relax to the ground state with rate k_{20} (k_{30}). Carriers in state $|1\rangle$ can radiatively relax to the ground state with rate k_{r} . In the model, we stipulate that carriers cannot be directly excited to state $|1\rangle$, because the energy of the fundamental is lower than the observed experimental emission, but must be excited to state $|2\rangle$ or $|3\rangle$ through multiphoton absorption. The interferometric nonlinear optical signal from this system was modeled through a density matrix approach, as described in the Methods.

We find that the model described above can reproduce the features of the experimental data when the population inversion of $|2\rangle$ is increased and states $|2\rangle$ and $|3\rangle$ both contribute to the radiative state $|1\rangle$, giving insight into the mechanism of the higher-order nonlinearities observed in the

coherent and incoherent emission of redox-exfoliated MoS₂. Figure 4 shows the comparison of the experimental and modeled SHG signal. The model reproduces the decrease in SHG intensity around τ_0 , as well as the asymmetries in the interferometric signal and the peaks at 3ω and 4ω in the Fourier transform spectrum. Experimental and modeled SHG interferograms are shown in Figure 4a and b, respectively. Experimental 2-D excitation/frequency detection correlation maps (Figure 4c) are also reproduced by modeling (Figure 4d). In addition, the integrated FT intensities obtained from experimental interferograms (Figure 4e) were reproduced by modeling (Figure 4f). Also, in agreement with the experimental results, the modeled interferograms have a power dependence, with the high-order nonlinearities becoming more prominent at higher powers. The high-order nonlinearities decreased SHG intensity near τ_0 observed in the modeled SHG signal can be explained as saturation of SHG signal as the population difference in states $|0\rangle$ and $|2\rangle$, $\rho_{22}-\rho_{00}$ (referred to in the optical Bloch formalism as the inversion) increases. This can be observed in Figure 4g, which shows the relationship between the inversion and SHG intensity, calculated for the first half cycle ($\tau = 0$ to $1/\omega$) for a series of interferograms simulated using different excitation powers. As expected from eq S9, the rate of transition between the ground state and resonant harmonic state (state |2)) decreases when the inversion increases. This observation suggests that a saturation of the SHG signal due to an increase in the value of $\rho_{22} - \rho_{00}$ is responsible for the high-order nonlinearities observed in the SHG of redox-exfoliated MoS₂. This explanation is also supported by the power-dependent data shown in Figure 2a, which exhibits signatures of saturation at high powers. Discrepancies between the model and experimental data may arise from the simplifying assumptions in the model of a transform-limited Gaussian pulse profile and the coherence times chosen for the various levels of the model.

Modeling also provides insight into the features of the MPPL photoluminescent signal. In the model, both twophoton and *n*-photon absorption to states $|2\rangle$ and $|3\rangle$ can contribute to the population of state |1), which is radiative. Based on the observation of peaks up to 10th order in the experimental FT spectrum, we choose n = 10 to model the results shown in Figure 5 and optimizing the relative weights of the 2- and 10-photon absorption by varying the transition matrix moments μ_{02} and μ_{03} . As discussed above, photoluminescence originating solely from 2 or 10 photon absorption cannot reproduce the experimental interferograms, indicating the contribution of a mixture of photon-orders. The Fourier transform spectrum of this model with mixed-order multiphoton absorption also qualitatively reproduces the features of the experimental spectra (Figure 5). However, differences in the relative amplitudes of the Fourier transform peaks between experiment and modeling may suggest that more multiphoton absorption processes may also contribute along with the 2- and 10-photon cases considered in the model. While the high-order peaks in the FT spectrum can be reproduced by a model that includes saturation of the multiphoton absorption similar to what was proposed for the SHG-detected FT spectrum, the time-domain interferogram for this case is not consistent with the experimental observation.

Influence of POMs on the Nonlinear Response of Nanomaterials. Comparison of the results from TMDs prepared by redox-exfoliation and metalorganic chemical vapor

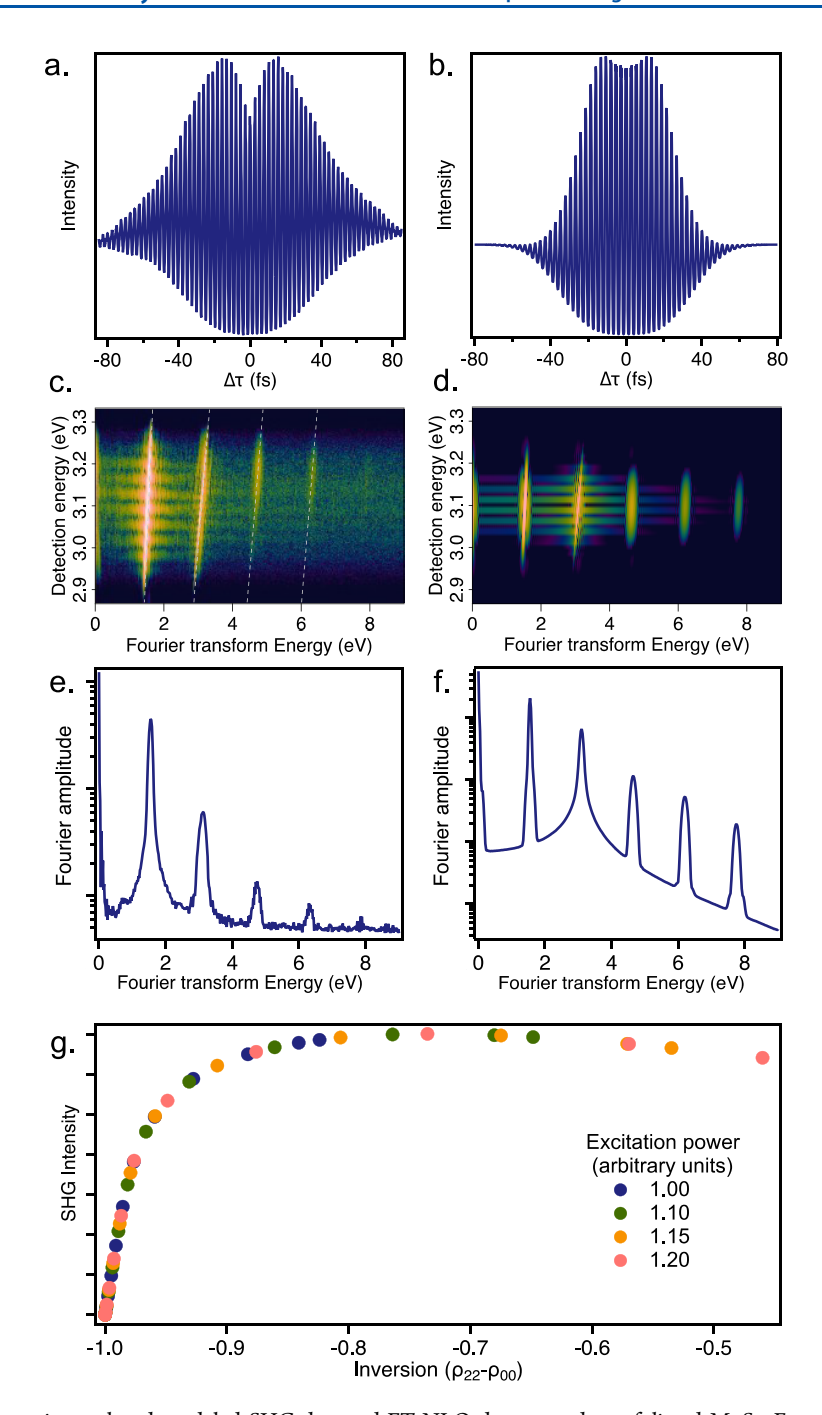


Figure 4. Comparison of experimental and modeled SHG-detected FT-NLO data on redox-exfoliated MoS₂. Experimental (a) and modeled (b) interferogram. Experimental (c) and modeled (d) 2-D excitation/detection frequency map. Experimental (e) and modeled (f) integrated FT spectrum. (g) Relationship between modeled SHG intensity and population inversion for the first cycle of the modeled interferogram performed with different excitation powers.

deposition (MOCVD) implicate the synthesis method in the saturable SHG and high-order MPPL described above. Monolayer and bilayer MOCVD-grown MoS₂ does not exhibit the high-order nonlinearities observed in redox-exfoliated MoS₂. Our analysis is limited to the SHG emission because no detectable MPPL was observed from MOCVD MoS₂ under our experimental conditions, possibly due to our detection window which is limited to <1.8 eV. The SHG-detected FT spectrum of MOCVD MoS₂ does not exhibit higher-order peaks indicative of saturation effects as discussed previously (Figure S3). However, redox-exfoliated WS₂ has a similar

nonlinear emission spectrum to redox-exfoliated MoS_2 and exhibits both high-order MPPL and saturable SHG (Figure S4). This suggests the importance of the redox-exfoliation method in influencing the nonlinear optical properties of TMDs.

We hypothesized that POM species formed during the TMD synthesis were responsible for the differences in the nonlinear optical response of redox-exfoliated TMDs compared to CVD-grown samples. Mild oxidation of TMD powders leads to the formation of soluble metal-oxide precursors (MOPs), which adsorb to the surface of the

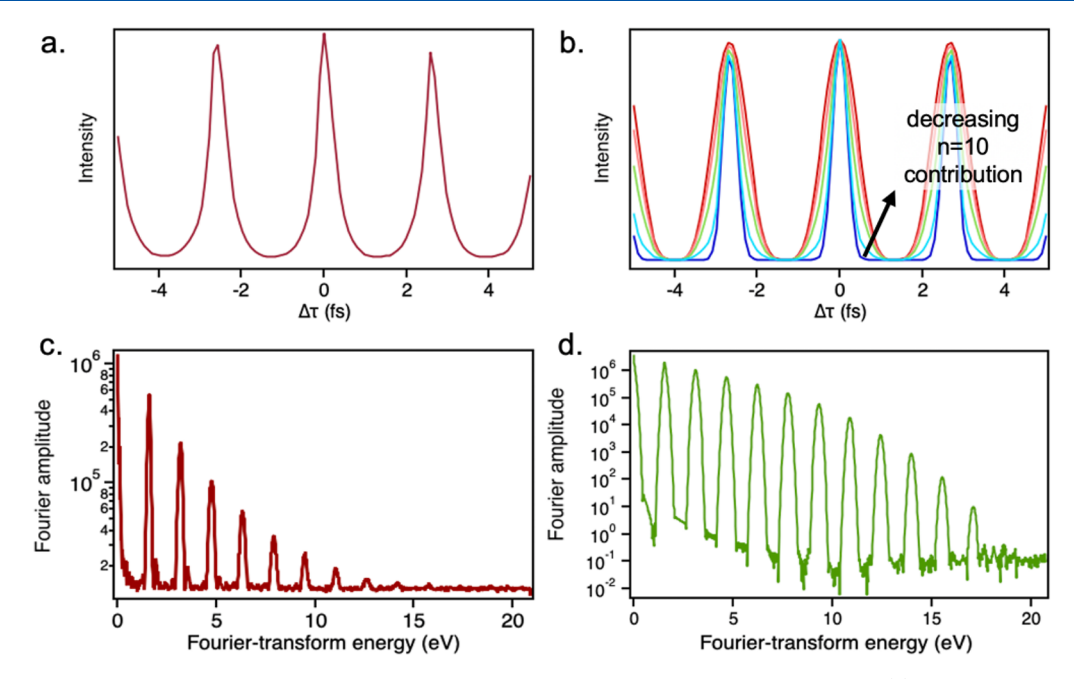


Figure 5. Comparison of experimental and modeled MPPL-detected FT-NLO data on redox-exfoliated MoS_2 . (a) Experimental interferogram; (b) series of interferograms modeled using a mixture of n = 2 and 10 contributions to the multiphoton absorption. (c, d) Experimental (c) and modeled (d) integrated FT spectra.

TMD crystals. Upon the addition of a reducing agent, MOPs assemble to form POM clusters, which drive the delamination of TMD crystals through Coulombic repulsion.¹² The resulting TMD flakes have an average thickness of under 3 nm and lateral dimensions of about 100–200 nm (Figures S5 and S6). These species adsorb onto the TMD flakes, and thus are likely present in the redox-exfoliated samples studied above.

To confirm the role of POMs in the high-order nonlinearities observed in redox-exfoliated TMDs, we studied other semiconductors decorated with POMs. Oxidation of MoS₂ with a mild oxidant affords soluble MOP precursors. These MOP precursors are separated from bulk MoS₂ powders and can be assembled via addition of a reducing agent. After addition of reductant, the MOPs assemble into macroanionic POM species. These assembled POMs were then dropcast on films of colloidal CdSe nanocrystals to study their effects on the nonlinear optical properties. Before the addition of POMs, the CdSe nanocrystals exhibit strong MPPL through the 1s exciton state at approximately 2.2 eV, along with SHG at 3 eV (Figure 6a). FT-NLO spectroscopy confirms that the SHG and MPPL are second and third-order nonlinear signals, respectively (Figure 6b,c). After the addition of POMs, the MPPL from the CdSe exciton is quenched and photoluminescence is observed at lower energies, with the nonlinear emission spectrum (Figure 6a) appearing similar to that of redox-exfoliated MoS₂ and WS₂. Higher-order peaks indicative of saturation are observed in the SHG-detected FT spectrum (Figure 6b) and up to 10th-order peaks are present in the MPPL-detected FT spectrum (Figure 6c). High-order excitation is not observed in POMs alone, which exhibited weak second-order MPPL, and no SHG (Figure S7). These results suggest that the high-order nonlinear optical properties observed in redox-exfoliated TMDs can be generalized to other semiconductors through adsorption of molecular POM clusters.

The addition of POMs to other nanomaterials did not induce saturable SHG or high-order MPPL, giving insight into

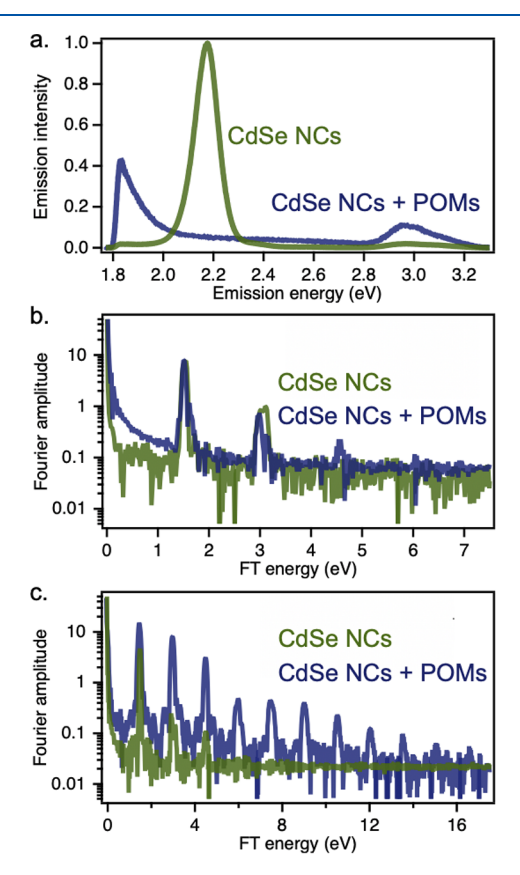


Figure 6. Nonlinear spectroscopy of CdSe/POMs. (a) Nonlinear emission spectra for CdSe nanocrystals with and without POMs. (b) SHG-detected Fourier transform spectra of CdSe nanocrystals with and without POMs. (c) MPPL-detected Fourier transform spectra of CdSe nanocrystals with and without POMs.

the mechanism of the nonlinear signals. Isolated POMs were added to films of metallic gold nanorods (AuNRs) and wide

bandgap hexagonal boronitride flakes (h-bn). FT-NLO spectroscopy demonstrates that AuNRs have third-order MPPL both before and after the addition of POMs (Figure S8). In h-bn, the SHG-detected FT spectra exhibit no saturation effects both before and after the addition of POMs (Figure S9). H-bn, which has been decorated with POMs, does exhibit a weak MPPL, which is not present in the pristine sample; however, this signal is only third-order based on FT measurements (Figure S9).

DISCUSSION

The combined experimental data and modeling results presented above demonstrate that redox-exfoliated MoS₂ exhibits rich nonlinear optical phenomena which are uniquely revealed by FT-NLO spectroscopy. Spectral resolution of the nonlinear emission allows the photophysical and chemical mechanisms of SHG saturation and MPPL to be examined. The SHG interferograms are reproduced by a simple model which suggests that the higher-order features observed in the Fourier transform spectra are consistent with saturation of the SHG intensity as the relative difference in population, or inversion, $\rho_{22}-\rho_{00}$, increases. The apparent 3rd to 4th-order power dependence of SHG is reproduced within the density matrix approach, suggesting that strong-field effects or nonperturbative high harmonic generation are not required to account for the multiphoton interactions. However, the observation of SHG saturation may imply that nonperturbative effects are necessary to fully reconcile the nonlinear response.

There are several potential mechanisms through which the increase in inversion can occur, depicted in Figure S10 as A, B, and C. In the first mechanism, A, there is a strong two-photon absorption resonant with a state at the harmonic energy, |2), which simultaneously increases ρ_{22} and decreases ρ_{00} , increasing the inversion. In mechanism B, while there must still be some finite population ρ_{22} , the inversion is increased mainly by the strong *n*-photon absorption to state $|3\rangle$, which depletes the ground state population, ρ_{00} . Finally, mechanism C depicts the case where carriers are excited mainly to state | 3), but a fast (within the duration of the laser pulse) carrier transfer to state |2| increases the inversion. Based on the results of the present study, we cannot conclusively assign a mechanism. However, mechanism B appears less likely than the other two options, since depletion of carriers in the ground state can be expected to result in saturation of the MPPL signal, which is not observed. Also, although mechanism A is plausible, the appearance of high-order MPPL and SHG saturation effects under the same experimental conditions suggests that the higher lying state |3\) may be involved in the SHG saturation mechanism, as in mechanism C.

Consideration of the results for CdSe nanocrystals, AuNRs, and h-bn also yield insights into the mechanisms of high-order nonlinearities in POM-decorated nanomaterials. We note that all of the mechanisms presented in Figure S10 require that state $|2\rangle$ is real in-order to have saturable SHG. MoS₂, CdSe nanocrystals, and AuNRs all have resonances at 2ω . The bandgap of h-bn, however, is approximately 6 eV, which is larger than the harmonic energy. The lack of saturable SHG in POM-doped h-bn is consistent with our model which requires a real state resonant with the harmonic frequency. The presence of third-order MPPL in the POM/h-bn sample suggests that this state is also important for allowing the high-order excitation observed in TMDs and CdSe. A further consideration for the excitation scheme is that in order to

achieve efficient multiphoton absorption as is observed in our MPPL data, real resonances at $n\omega$ are likely needed. These resonances could be provided by either the semiconductor or the POM clusters.

Based on the nonlinear emission spectra of CdSe, MoS₂, and WS₂, we attribute the MPPL emission to radiative recombination by the surface-adsorbed POM cluster. The quenching of the CdSe exciton emission upon addition of the POMs suggests charge transfer from CdSe to the POMs. This is consistent with literature reports of POMs behaving as electron acceptors.^{33,34} While electron transfer may occur in either direction at equilibrium depending on the relative alignment of the CdSe and POMs Fermi levels, the observation of CdSe photoluminescence quenching suggests that the POMs act as an acceptor for excited carriers. The similar emission for MoS₂ and WS₂ compared to the POMs emission (Figure S7) suggests that a similar charge transfer mechanism also occurs in the TMD/POMs systems. In contrast, we expect electron transfer to the POMs from AuNRs to be much less likely; gold nanoparticles are typically photoluminescence quenchers.³⁵ This may explain why AuNR/POM samples do not exhibit high-order nonlinearities, despite the 2ω resonance with the AuNR interband transition. Taken together, the photophysical and chemical mechanisms described here highlight the importance of both the semiconductor and the surfaceadsorbed POMs for influencing the nonlinear optical properties of these solution-exfoliated heterostructures. The 2ω resonant MoS₂ C-transition provides an efficient pathway for SHG and multiphoton excitation, and the electron accepting POMs enable an increase of the population inversion in the heterostructure. Combined with efficient high-order photon absorption, the synergistic nonlinear optical and charge transfer characteristics of the composite POM/MoS₂ system are responsible for the optical properties described in this

The high-order nonlinear optical phenomena described in this work are unusual to observe in the perturbative regime. The 10th-order MPPL in redox-exfoliated MoS₂ described here is to our knowledge the highest photon order observed in the perturbative regime using a NIR laser fundamental. Previous work has demonstrated 11-photon absorption at the bandgap of chalcogenide glasses using laser wavelengths in the mid-IR.³⁶ The high-order MPPL observed in this work is unique in that it suggests excitation energies above 15 eV, which is far above the bandgap and even the ionization potential of few-layer TMDs and CdSe nanocrystals.^{37–39} This observation was enabled by the use of FT-NLO spectroscopy, which revealed 10th-order excitation that was obscured in the excitation power dependence; the steady-state power dependence only reports on the average photon-order. FT-NLO spectroscopy allowed us to resolve high-order excitation, despite strong contributions at lower photon-orders due to real material resonances that exist due to 2ω being above the bandgap threshold.

In addition to high-order MPPL, we observed saturable SHG. Previous studies have shown that saturable SHG can be observed in quantum wells, 40,41 nanopatterned dielectric/metal structures, 42 and ZnO nanoparticles. 43 Previous work has discussed saturable SHG in the context of limitations on the performance of multiple quantum well structures for intersubband SHG. However, saturable SHG, as a wave mixing analogue to saturable absorption, could have implications for applications including pulse shaping and optical limiting

technologies. This work demonstrates that saturable SHG can be straightforwardly induced in semiconducting nonlinear optical materials through the addition of POMs.

CONCLUSIONS

The nonlinear optical properties of redox-exfoliated MoS2 were studied with Fourier transform spectroscopy, revealing highorder multiphoton absorption and saturable second harmonic generation. Through examination and modeling of the nonlinear interferograms, these high-order signals in the excitation spectra were understood to originate from mixedorder excitation, resulting in MPPL up to and including 10th order. High-order excitation was also implicated as one component that resulted in saturable second harmonic generation. These effects arise through the formation of POM-cluster adsorbates during the redox-exfoliation process for TMDs. The surface-adsorbed POMs provide a critical electron accepting function, that are essential to increasing the population inversion in the material heterostructure. These results demonstrate the importance of synthetic method and material composition in determining the structure and properties of 2D materials. The ability of POM adsorption to generate high-order MPPL and saturated SHG is generalizable to other semiconducting nanomaterials with resonantly enhanced SHG, indicating an avenue to easily alter the nonlinear optical and electronic properties of nanomaterials for sensing, optical limiting technologies, electrochemical, and integrated photonic circuits.

This study also demonstrates the power of Fourier transform based nonlinear optics for understanding the optical and electronic properties of complex materials. The high-order effects in both SHG and MPPL were obscured by conventional power-dependent studies, and uniquely observed using Fourier transform methods. The use of interferometric Fourier transform nonlinear optical spectroscopy has potential to resolve important multiphoton excitation and chemical charge transfer mechanisms that may be obscured by conventional imaging techniques. Therefore, the Fourier transform methods described here can have impacts in resolving both photophysical and chemical mechanisms that underlie function in many photonic materials.

ASSOCIATED CONTENT

Supporting Information

The Supporting Information is available free of charge at https://pubs.acs.org/doi/10.1021/acs.jpcc.2c05739.

Description of the FT-NLO simulation approach and Figures S1-S10 (PDF)

AUTHOR INFORMATION

Corresponding Author

Kenneth L. Knappenberger, Jr. — Department of Chemistry, Pennsylvania State University, University Park, Pennsylvania 16802, United States; Oorcid.org/0000-0003-4123-3663; Email: klk260@psu.edu

Authors

Megan A. Steves — Department of Chemistry, Pennsylvania State University, University Park, Pennsylvania 16802, United States; © orcid.org/0000-0002-1410-5650

- Ali Jawaid Materials and Manufacturing Directorate, Air Force Research Laboratory, Wright-Patterson AFB, Dayton, Ohio 45433-7702, United States
- Ariel Struzyk Department of Chemistry, Pennsylvania State University, University Park, Pennsylvania 16802, United States
- Riccardo Torsi Department of Materials Science and Engineering, Pennsylvania State University, University Park, Pennsylvania 16802, United States; orcid.org/0000-0001-7748-1074
- Joshua A. Robinson Department of Materials Science and Engineering, Pennsylvania State University, University Park, Pennsylvania 16802, United States; 2D Crystal Consortium, Materials Research Institute and Center for 2D and Layered Materials, Pennsylvania State University, University Park, Pennsylvania 16802, United States
- Richard A. Vaia Materials and Manufacturing Directorate, Air Force Research Laboratory, Wright-Patterson AFB, Dayton, Ohio 45433-7702, United States; orcid.org/ 0000-0003-4589-3423

Complete contact information is available at: https://pubs.acs.org/10.1021/acs.jpcc.2c05739

Author Contributions

The manuscript was written through contributions of all authors. All authors have given approval to the final version of the manuscript.

Notes

The authors declare no competing financial interest.

ACKNOWLEDGMENTS

This work was supported by a grant from the U.S. Air Force Office of Scientific Research, Grant Number FA-9550-18-1-0347. Support from the National Science Foundation (Award Numbers CHE-1807999 and DGE1255832) is also acknowledged.

REFERENCES

- (1) Fejer, M. M. Nonlinear Optical Frequency Conversion. *Phys. Today* **1994**, 47 (5), 25–32.
- (2) Farsari, M.; Vamvakaki, M.; Chichkov, B. N. Multiphoton Polymerization of Hybrid Materials. *Journal of Optics* **2010**, *12* (12), 124001.
- (3) LaFratta, C. N.; Fourkas, J. T.; Baldacchini, T.; Farrer, R. A. Multiphoton Fabrication. *Angew. Chem., Int. Ed.* **2007**, *46* (33), 6238–6258.
- (4) Zipfel, W. R.; Williams, R. M.; Webb, W. W. Nonlinear Magic: Multiphoton Microscopy in the Biosciences. *Nat. Biotechnol.* **2003**, *21* (11), 1369–1377.
- (5) Miras, H. N.; Yan, J.; Long, D.-L.; Cronin, L. Engineering Polyoxometalates with Emergent Properties. *Chem. Soc. Rev.* **2012**, *41* (22), 7403.
- (6) Ueda, T. Electrochemistry of Polyoxometalates: From Fundamental Aspects to Applications. *ChemElectroChem.* **2018**, 5 (6), 823–838.
- (7) Kang, Z.; Tsang, C. H. A.; Zhang, Z.; Zhang, M.; Wong, N. B.; Zapien, J. A.; Shan, Y.; Lee, S. T. A Polyoxometalate-Assisted Electrochemical Method for Silicon Nanostructures Preparation: From Quantum Dots to Nanowires. J. Am. Chem. Soc. 2007, 129 (17), 5326–5327.
- (8) Troupis, A.; Hiskia, A.; Papaconstantinou, E. Synthesis of Metal Nanoparticles by Using Polyoxometalates as Photocatalysts and Stabilizers. *Angew. Chem., Int. Ed.* **2002**, *41* (11), 1911.

- (9) Jawaid, A.; Che, J.; Drummy, L. F.; Bultman, J.; Waite, A.; Hsiao, M.-S.; Vaia, R. A. Redox Exfoliation of Layered Transition Metal Dichalcogenides. *ACS Nano* **2017**, *11* (1), 635–646.
- (10) Al-Yasari, A.; Van Steerteghem, N.; Kearns, H.; El Moll, H.; Faulds, K.; Wright, J. A.; Brunschwig, B. S.; Clays, K.; Fielden, J. Organoimido-Polyoxometalate Nonlinear Optical Chromophores: A Structural, Spectroscopic, and Computational Study. *Inorg. Chem.* **2017**, *56* (17), 10181–10194.
- (11) Hassan, S. ul; Zhou, Y.; Zhang, L.; Shi, Z.; Yang, D.; Asif, H. M.; Qu, N. Remarkable Enhancement in the Nonlinear Optical Responses of Porphyrins Realized by Combination with Polyoxometalates via Covalent Bonding: A Case Study. *J. Phys. Chem. C* **2016**, *120* (14), 7757–7766.
- (12) Jawaid, A. M.; Ritter, A. J.; Vaia, R. A. Mechanism for Redox Exfoliation of Layered Transition Metal Dichalcogenides. *Chem. Mater.* **2020**, 32 (15), 6550–6565.
- (13) Zhang, M.; Han, N.; Wang, J.; Zhang, Z.; Liu, K.; Sun, Z.; Zhao, J.; Gan, X. Strong Second Harmonic Generation from Bilayer Graphene with Symmetry Breaking by Redox-Governed Charge Doping. *Nano Lett.* **2022**, 22 (11), 4287–4293.
- (14) Jiang, P.; Zhang, B.; Liu, Z.; Chen, Y. MoS ₂ Quantum Dots Chemically Modified with Porphyrin for Solid-State Broadband Optical Limiters. *Nanoscale* **2019**, *11* (43), 20449–20455.
- (15) Rakovich, A.; Nabiev, I.; Sukhanova, A.; Lesnyak, V.; Gaponik, N.; Rakovich, Y. P.; Donegan, J. F. Large Enhancement of Nonlinear Optical Response in a Hybrid Nanobiomaterial Consisting of Bacteriorhodopsin and Cadmium Telluride Quantum Dots. *ACS Nano* 2013, 7 (3), 2154–2160.
- (16) Sanusi, K.; Khene, S.; Nyokong, T. Enhanced Optical Limiting Performance in Phthalocyanine-Quantum Dot Nanocomposites by Free-Carrier Absorption Mechanism. *Opt Mater.* **2014**, *37*, 572–582.
- (17) Mak, K. F.; Lee, C.; Hone, J.; Shan, J.; Heinz, T. F. Atomically Thin MoS_{22} : A New Direct-Gap Semiconductor. *Phys. Rev. Lett.* **2010**, 105 (13), 136805.
- (18) Sallen, G.; Bouet, L.; Marie, X.; Wang, G.; Zhu, C. R.; Han, W. P.; Lu, Y.; Tan, P. H.; Amand, T.; Liu, B. L.; et al. Robust Optical Emission Polarization in MoS₂ Monolayers through Selective Valley Excitation. *Phys. Rev. B* **2012**, *86* (8), 081301.
- (19) Mak, K. F.; He, K.; Shan, J.; Heinz, T. F. Control of Valley Polarization in Monolayer MoS₂ by Optical Helicity. *Nat. Nano-technol.* **2012**, 7 (8), 494–498.
- (20) Ugeda, M. M.; Bradley, A. J.; Shi, S.-F.; da Jornada, F. H.; Zhang, Y.; Qiu, D. Y.; Ruan, W.; Mo, S.-K.; Hussain, Z.; Shen, Z.-X.; et al. Giant Bandgap Renormalization and Excitonic Effects in a Monolayer Transition Metal Dichalcogenide Semiconductor. *Nat. Mater.* **2014**, *13* (12), 1091–1095.
- (21) Autere, A.; Jussila, H.; Dai, Y.; Wang, Y.; Lipsanen, H.; Sun, Z. Nonlinear Optics with 2D Layered Materials. *Adv. Mater.* **2018**, *30*, 1705963.
- (22) Malard, L. M.; Alencar, T. V.; Barboza, A. P. M.; Mak, K. F.; De Paula, A. M. Observation of Intense Second Harmonic Generation from MoS₂ Atomic Crystals. *Physical Review B Condensed Matter and Materials Physics* **2013**, 87 (20), 201401.
- (23) Rukelj, Z.; Strkalj, A.; Despoja, V. Optical Absorption and Transmission in a Molybdenum Disulfide Monolayer. *Phys. Rev. B* **2016**, *94*, 115428.
- (24) Maldonado, M. E.; Das, A.; Jawaid, A. M.; Ritter, A. J.; Vaia, R. A.; Nagaoka, D. A.; Vianna, P. G.; Seixas, L.; de Matos, C. J. S.; Baev, A.; et al. Nonlinear Optical Interactions and Relaxation in 2D Layered Transition Metal Dichalcogenides Probed by Optical and Photoacoustic Z-Scan Methods. *ACS Photonics* **2020**, *7* (12), 3440–3447.
- (25) Silva-Neto, M. L.; Maldonado, M.; de S. Menezes, L.; de Araújo, C. B.; Jawaid, A. M.; Busch, R.; Ritter, A. J.; Vaia, R. A.; Gomes, A. S. L. Fifth-Order Optical Nonlinear Response of Semiconducting 2D LTMD MoS₂. Opt. Lett. **2021**, 46 (3), 226–229. (26) Maldonado, M.; da Silva Neto, M. L.; Vianna, P. G.; Ribeiro, H. B.; de Araújo, C. B.; Matos, C. J. S. de; Seixas, L.; Jawaid, A. M.; Busch, R.; Ritter, A. J.; et al. Femtosecond Nonlinear Refraction of 2D

- Semi-Metallic Redox Exfoliated ZrTe₂ at 800 nm. Appl. Phys. Lett. 2021, 118 (1), 011101.
- (27) Paul, S.; Torsi, R.; Robinson, J. A.; Momeni, K. Effect of the Substrate on MoS 2 Monolayer Morphology: An Integrated Computational and Experimental Study. ACS Appl. Mater. Interfaces 2022, 14 (16), 18835–18844.
- (28) Stevenson, P. R.; Busch, R. T.; Torsi, R.; Jawaid, A. M.; Rao, R.; Lioi, D. B.; Robinson, J. A.; Glavin, N. R.; Vaia, R. A.; Kennedy, W. J.; Vernon, J. P. Reversibly Tailoring Optical Constants of Monolayer Transition Metal Dichalcogenide MoS₂ Films: Impact of Dopant-Induced Screening from Chemical Adsorbates and Mild Film Degradation. ACS Photonics 2021, 8 (6), 1705–1717.
- (29) Steves, M. A.; Knappenberger, K. L. Achieving Sub-Diffraction Spatial Resolution Using Combined Fourier Transform Spectroscopy and Nonlinear Optical Microscopy. *J. Chem. Phys.* **2022**, *156* (2), 021101.
- (30) Jarrett, J. W.; Zhao, T.; Johnson, J. S.; Knappenberger, K. L. Investigating Plasmonic Structure-Dependent Light Amplification and Electronic Dynamics Using Advances in Nonlinear Optical Microscopy. J. Phys. Chem. C 2015, 119 (28), 15779—15800.
- (31) Stibenz, G.; Steinmeyer, G. Interferometric Frequency-Resolved Optical Gating. Opt. Express 2005, 13 (7), 2617.
- (32) Schmidt, S.; Mascheck, M.; Silies, M.; Yatsui, T.; Kitamura, K.; Ohtsu, M.; Lienau, C. Distinguishing between Ultrafast Optical Harmonic Generation and Multi-Photon-Induced Luminescence from ZnO Thin Films by Frequency-Resolved Interferometric Autocorrelation Microscopy. *Opt. Express* **2010**, *18* (24), 25016.
- (33) Singh, D. P.; Pandey, S.; Gupta, S. K.; Manohar, R.; Daoudi, A.; Sahraoui, A. H.; Phadnis, C.; Mahamuni, S. Quenching of Photoluminescence and Enhanced Contrast of Ferroelectric Liquid Crystal Dispersed with Cd₁-XZnXS/ZnS Core/Shell Nanocrystals. *J. Lumin.* **2016**, *173*, 250–256.
- (34) Pramata, A. D.; Suematsu, K.; Quitain, A. T.; Sasaki, M.; Kida, T. Synthesis of Highly Luminescent SnO₂ Nanocrystals: Analysis of Their Defect-Related Photoluminescence Using Polyoxometalates as Quenchers. *Adv. Funct. Mater.* **2018**, 28 (4), 1704620.
- (35) Yun, C. S.; Javier, A.; Jennings, T.; Fisher, M.; Hira, S.; Peterson, S.; Hopkins, B.; Reich, N. O.; Strouse, G. F. Nanometal Surface Energy Transfer in Optical Rulers, Breaking the FRET Barrier. *J. Am. Chem. Soc.* **2005**, *127* (9), 3115–3119.
- (36) Sohn, B. U.; Kang, M.; Choi, J. W.; Agarwal, A. M.; Richardson, K.; Tan, D. T. H. Observation of Very High Order Multi-Photon Absorption in GeSbS Chalcogenide Glass. *APL Photonics* **2019**, *4* (3), 36102.
- (37) Keyshar, K.; Berg, M.; Zhang, X.; Vajtai, R.; Gupta, G.; Chan, C. K.; Beechem, T. E.; Ajayan, P. M.; Mohite, A. D.; Ohta, T. Experimental Determination of the Ionization Energies of MoSe₂, WS₂, and MoS₂ on SiO₂ Using Photoemission Electron Microscopy. ACS Nano **2017**, 11 (8), 8223–8230.
- (38) Meulenberg, R. W.; Lee, J. R. I.; Wolcott, A.; Zhang, J. Z.; Terminello, L. J.; van Buuren, T. Determination of the Exciton Binding Energy in CdSe Quantum Dots. *ACS Nano* **2009**, 3 (2), 325–330.
- (39) Brus, L. E. A Simple Model for the Ionization Potential, Electron Affinity, and Aqueous Redox Potentials of Small Semi-conductor Crystallites. *J. Chem. Phys.* **1983**, 79 (11), 5566–5571.
- (40) Boucaud, P.; Rosencher, E.; Bois, P.; Julien, F. H.; Yang, D. D.; Lourtioz, J.-M. Saturation of Second-Harmonic Generation in GaAs-AlGaAs Asymmetric Quantum Wells. *Opt. Lett.* **1991**, *16* (4), 199.
- (41) Gomez-Diaz, J. S.; Tymchenko, M.; Lee, J.; Belkin, M. A.; Aìu, A. Nonlinear Processes in Multi-Quantum-Well Plasmonic Metasurfaces: Electromagnetic Response, Saturation Effects, Limits, and Potentials. *Phys. Rev. B* **2015**, *92*, 125429.
- (42) Zhang, J.; Wang, L.; Krishna, S.; Sheik-Bahae, M.; Brueck, S. R. J. Saturation of the Second Harmonic Generation from GaAs-Filled Metallic Hole Arrays by Nonlinear Absorption. *Phys. Rev. B* **2011**, 83, 165438.
- (43) Dai, J.; Dai, Q.-F.; Zeng, J.-H.; Lan, S.; Wan, X.; Tie, S.-L. Negative Slope for Second Harmonic Generation Observed at High

Excitation Intensities in ZnO Nanorods. IEEE J. Quantum Electron. 2013, 49 (11), 903-909.

Recommended by ACS

Valley Relaxation of the Moiré Excitons in a WSe₂/MoSe₂ Heterobilayer

Keisuke Shinokita, Kazunari Matsuda, et al.

SEPTEMBER 28, 2022

ACS NANO

READ

Probing Spin Dynamics of 2D Excitons with Twisted Light

Aswini Kumar Pattanayak, Sajal Dhara, et al.

OCTOBER 07, 2022

ACS PHOTONICS

READ 🗹

Probing Nanoscale Exciton Funneling at Wrinkles of Twisted Bilayer MoS₂ Using Tip-Enhanced Photoluminescence **Microscopy**

Jiaqi Shao, Hong-Wei Lu, et al.

APRIL 07, 2022

THE JOURNAL OF PHYSICAL CHEMISTRY LETTERS

READ 🗹

Electrically Tunable Localized versus Delocalized Intralayer Moiré Excitons and Trions in a Twisted MoS₂ Bilayer

Medha Dandu, Kausik Majumdar, et al.

JUNE 09, 2022

ACS NANO

READ

Get More Suggestions >